

HOT SPOTS IN CYGNUS A; A MOSAICED MAP AT 86 GHz

M.C.H. Wright

Radio Astronomy Laboratory, University of California, Berkeley

R.J. Sault

National Center for Supercomputing Applications, University of Illinois,
Urbana-Champaign

ABSTRACT We describe a new software package, MIRIAD, for making multichannel images of multiple-field aperture synthesis observations. As an example of the use of the new software we present a map of the radio galaxy Cygnus A. We used the BIMA array to map Cygnus A at 86 GHz with 2.28×3.06 arcsec resolution in 3 fields centered on the central radio source and the radio hot spots in each radio lobe. The 3 fields were combined and deconvolved to find the positions and flux densities of the radio source components.

INTRODUCTION

The BIMA millimeter wavelength array has been used previously to map the radio source Cygnus A. These observations, with limited dynamic range, showed that the hot spots in the radio lobes have straight spectral indices $0.98 + / - 0.02$, significantly flatter than the lobe emission. No features corresponding to electron aging were found, implying a continuing supply of energy to both lobes. This result has been confirmed by observations at even higher frequencies at the JCMT (Eales, Duncan and Alexander, 1990).

If the hot spots represent the places where relativistic particles are generated, then we may expect to find differences in the spectra of the hot spots within each radio lobe. None of the millimeter observations have sufficient resolution to distinguish between the hot spots in each radio lobe. These are separated by a few arcsec, and are in principle resolvable with the BIMA array.

Care must be taken with the observations and data reduction techniques because Cygnus A spans 2 arcminutes in the sky, close to the half power beamwidth of the BIMA antennas, and the observations must have sufficient dynamic range to separate the multiple hot spots which may have widely different fluxes at high frequencies.

Many radio sources are larger than the primary beamwidth of the antennas at millimeter wavelengths and observations of multiple pointing centers are often required for aperture synthesis observations. An additional

complication arises for spectral line observations. The signal is distributed over many spectral line channels, and for self-calibration all the channels must be used in determining the source distribution which best fits the data.

Faced with these problems for multichannel image reconstruction, we have written a new software package, MIRIAD, which would facilitate the development of new algorithms. This package is specifically intended to cope with multichannel images, formed from multiple pointings. Because of the size and structure of Cygnus A, observations of this source provide an excellent test of the new software.

In this paper we describe the observations and reduction techniques used to obtain a map of Cygnus A with 2.28×3.06 arcsec resolution and a dynamic range (peak/rms) of 175.

OBSERVATIONS AND DATA REDUCTION

We used the BIMA 3-element millimeter array to map Cygnus A at 86 GHz. The data were obtained in a single 12-hour observation on 26 Feb 1990. The antennas were pointed in turn towards each of 3 fields centered on the central radio source and the hot spots in each radio lobe. Since the halfpower beamwidth of the 6m antennas is 2.3 arcmin at 86 GHz, we fully map the radio emission from Cygnus A with 3 fields separated by 1 arcmin. The antenna were positioned along an east-west line with separations of 73, 122 and 195m. The synthesised beamwidth is 2.28×3.06 arcsec. Because of the minimum antenna separation used, structure larger than 12 arcsec is not completely sampled, and the extended radio lobes are not represented in the maps presented.

The data were calibrated by observations of the quasar 2005+403 whose flux density was determined to be 1.5 Jy from observations of Mars.

The antenna gains were determined using the self-calibration procedure in MIRIAD by a least squares fit to a point source with the a-priori position and flux density assumed for 2005+403. This procedure is equivalent to the customary fitting of amplitudes and phases to the calibrator data, but with the advantages that the data are properly weighted according to the signal to noise ratio, and that phase closure, and 2π phase ambiguities are automatically handled. The time scale in the self-calibration was set equal to the calibration interval of 45 minutes. The gains derived from the calibrator were then applied to the observations of Cygnus A. The 3 fields of Cygnus A were cleaned using the Hogbom algorithm, and combined using a linear mosaicing algorithm. This combination process corrects for primary beam attenuation, and weights pixels so as to minimise the mean square error in the resultant map (i.e. the combination is optimum in the Weiner sense). The restored map is shown in Figure 1.

The central radio source and hot spots are clearly evident on this map. Since the instrumental phase stability and weather were quite good, the a-priori calibration gives an rms noise level of 20 mJy, close to that calculated from the receiver noise. These results were checked with a more conventional calibration procedure.

The rms noise level was further reduced by using this mosaiced map as a model for self-calibration in order to remove atmospheric phase fluctuations

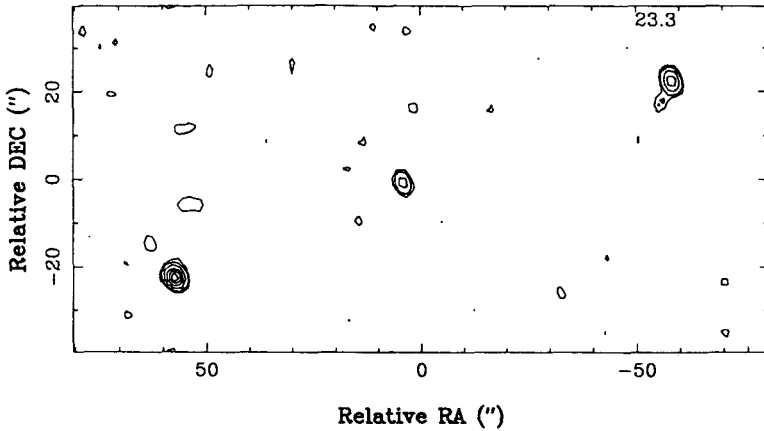


Fig. 1. Cygnus A. Mosaic of Cleaned Maps.

on time scales shorter than the calibration interval. The time scale for the self-calibration was set to 5 minutes, so that all 3 fields were simultaneously used to determine the antenna gains.

The self-calibration algorithm performs a least squares fit by minimizing

$$\sum_k \sum_{i,j(i \neq j)} ((V'_{ij}(k) - g_i(k)g_j^*(k)V_{ij}(k)) / \sigma_{ij}(k))^2$$

Here g_i, g_j are the unknown antenna gains, V'_{ij} is the observed source visibility, and V_{ij} and the visibility computed from the model. σ is estimated from the receiver noise. The antenna gains are assumed to be independent of the pointing center and the frequency channel. Thus the summation can be taken over all the observed fields, and all frequency channels. In the case of the Cygnus A observations, the data comprises of 3 fields, and 2 wideband channels (the upper and lower sideband of the first local oscillator).

In order to use the mosaiced image as the model for the self-calibration, we first weight the model by the primary beam centered at the various pointing centers, and then use these multiple models and frequency channels in a simultaneous least squares solution for the antenna gains.

The resultant corrected visibilities were then remapped, cleaned and mosaiced. The restored image is given in Figure 2. This image shows a factor of 2 improvement in dynamic range.

RESULTS

The positions of the source components were measured from the mosaiced image with the a-priori calibration, and are thus measured with respect to the assumed position for 2005+403 (RA(1950)=20:05:59.56 DEC=40:21:01.80). Since 2005+403 is quite close to Cygnus A, phase errors due to errors in the

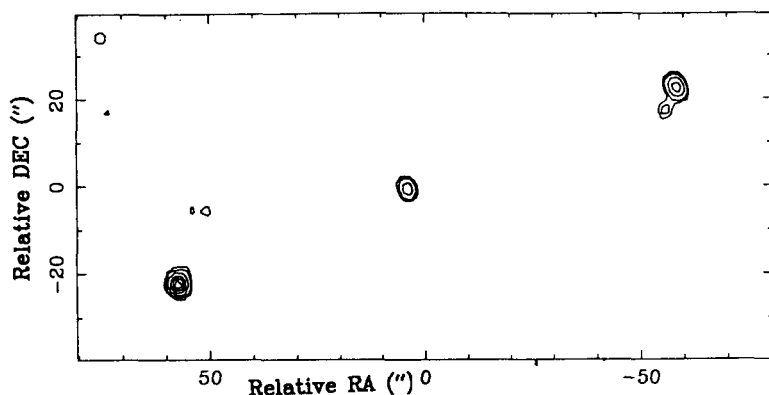


Fig. 2. Cygnus A. Mosaic after Self Calibration.

assumed baseline are very small. At 86 GHz, a baseline error, dB nanoseconds, leads to a phase error, $360 \times 86 \times \text{dB} \cdot \text{ds}$ degrees, where ds is the angle between source and calibrator. The baseline was determined in the usual way from observations of quasars with well determined positions. The error in the baseline, dB ~ 0.001 nanoseconds in each coordinate, so that the phase error due to baseline error ~ 0.5 degrees, much smaller than the atmospheric phase fluctuations of 5 - 10 degrees. The positions are good to about 0.1 of the synthesised beamwidth.

TABLE I

Positions and Flux Densities for Cygnus A Components

Component	RA	DEC	Flux density
A	19 57 38.97 (.03)	40 36 09.6 (.3)	2.17
B	19 57 39.15 (.05)	40 36 05.1 (.5)	0.4
Center	19 57 44.45 (.03)	40 35 46.1 (.3)	0.85
D	19 57 49.11 (.03)	40 35 24.8 (.3)	4.2

The positions are in excellent agreement with those given by Dreher (1981) at 22 GHz. The position for component B refers to the separate peak seen in Figure 1. Component B is much better defined than in the maps presented by Wright and Birkinshaw (1984), and the position given here is to be preferred.

The flux densities are measured from the restored image (Figure 1). The flux densities on the self-calibrated image (Figure 2) are about 10% higher. The flux densities given in Table 1 are the integrated fluxes within each source component, including the more diffuse emission surrounding the peaks. We

attributed 0.4 Jy to component B, out of a total 2.57 for the A/B component complex.

CONCLUSIONS

The multiple field observations of Cygnus A, and the imaging techniques used in the MIRIAD software have given a higher dynamic range image with a single 12 hour observation, than obtained with 10 baselines used in the previous observations with the same instrument.

REFERENCES

- Dreher, J.W., 1981, *A.J.*, 86, 833.
Eales, S.A., Duncan, W.D., and Alexander, P., 1990, Submillimeter Astronomy, eds. G.D.Watt and A.S.Webster, Kluwer Academic Publishers.
Wright, M.C.H., and Birkinshaw, M., 1984, *Ap.J.* 281, 135.